Electro-magnetic modeling of the planned active in-vessel coils at ASDEX Upgrade

M. Rott, U. Seidel, B. Streibl, W. Suttrop, T. Vierle, and the The ASDEX Upgrade Team
Max-Planck-Institut für Plasmaphysik, EURATOM Association, Boltzmannstrasse 2, D-85740 Garching, Germany

Abstract

A set of 16 in-vessel saddle coils is designed for mitigation of edge localised modes and feedback control of resistive wall modes in ASDEX Upgrade as part of a multi-stage enhancement for MHD control. The saddle coils are operated with direct and alternating currents. Substantial eddy currents are induced in the metal coil casing and an existing massive copper conductor near the coils mount position in the vacuum vessel. The shielding of the produced field, phase lag between coil current and produced field, active and apparent power, heating of the coil casing and re-cooling of the coil structure are modeled with 2D magnetodynamic and thermal finite element calculations. The results show that the design objectives (f = 500 Hz, dc normal field B_n = 6 mT, ac normal field B_n = 1 mT, pulse length $t_{\mathrm{pulse}} \geq 6$ s, cool-down time $t_{\mathrm{pause}} \leq 15$ min) are met or, in most cases, exceeded.

1. Introduction

It is planned to extend ASDEX Upgrade with a set of 24 in-vessel saddle coils, ac power supplies, a conducting wall and a feedback system for closed loop MHD control [1–4]. The first stage of the enhancement consists of 16 saddle coils with 5 turns mounted on the low field side above and below midplane at the two branches of the existing passive stabilising loop (PSL), a massive copper conductor used to slow down the vertical growth rate of the elongated ASDEX Upgrade plasmas. The mechanical design of these coils, their fixture on the PSL and the power and cooling water feeds are described in Ref. [5].

The coils have to be hermetically sealed to avoid breakdown and even arcs in the plasma chamber leading to short circuits of the turns and possible damage to the insulator. This is achieved with a full metal casing, which, however, allows ring eddy currents parallel and opposite to the winding current. In order to minimize the eddy currents and hence the magnetic field shielding the casing is made of a thin sheet of high resistive Ni-based material (alloy 600, inconel). However, the required coil current (I_{coil} = 1 kA) and consequently the $j \times B$ forces arising from operation during tokamak pulses define the minimum sheet thickness (1.2 mm, see Ref. [5]). In addition, the mounting distance to the PSL of the upper set of coils (termed `Bu`-coils) is limited to 10 mm by the need to avoid conflicts with the plasma cross-section. More space (30 mm) is left for the lower coils (`Bl`-coils). At the same time a wide frequency range of dc . . . 500 Hz is required for ELM suppression and RWM stabilisation [4]. Finally, dissipation in the passive conductors leads to Joule heating, which defines cooling and active power requirement. These demands call for a verification of the coil performance by electromagnetic and thermal computations which are the topic of the present paper.

Email address: `Michael.Rott@ipp.mpg.de` (M. Rott).

2. Electromagnetic simulations

The electromagnetic calculations are done with the `QuickField` [1] two-dimensional finite element code. The "ac magnetics" formulation is used, which - at a given frequency - solves for the complex magnetic vector potential A_z, i.e. the component perpendicular to the $x-y$ plane of the model. In a magnetodynamic approximation, the displacement current is set to zero, as for the frequency range considered (dc to a few 100 Hz) the electromagnetic wavelengths are much larger than the dimensions of the model. `QuickField` treats passive conductors (eddy currents only) as well as the current distribution in active conductors (skin effect) and allows to connect model regions with an external lumped circuit model to evaluate global quantities such as resistance and inductance.

2.1. *Finite element model*

The saddle coils have a length of about 1.7 m in toroidal direction and 0.3 m height (poloidal extent). The strong elongation and large radius of the toroidal curvature ($R < 2$ m, see Fig. 1) allows to apply a two-dimensional planar model, containing the cross-sections of the two toroidal branches (see Fig. 2).

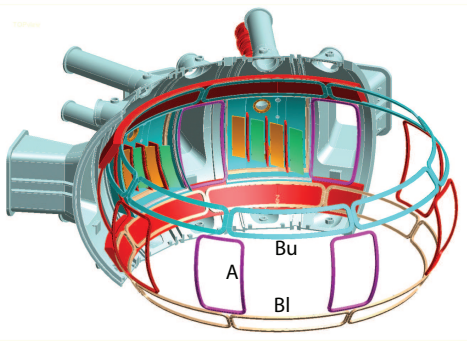

Fig. 1. Position of the coils inside the vessel of ASDEX Upgrade

Eddy currents in the stiffening ribs between coil top casing and baseplate [5] are negligible because the stiffeners are perpendicular to the current direction and their thickness (1.2 mm) is much less than the skin depth in alloy 600 in the frequency range considered here. Voltage drop, inductance and resistance of active conductors returned by `QuickField` correspond to 1 m length perpendicular to the model plane. In order to assess these parameters for the entire coil, a correction factor is used that is obtained from the analytical formula for the inductance of a rectangular coil [6], cross-checked with numerical inductance calculations with the `HEDO` code [7].

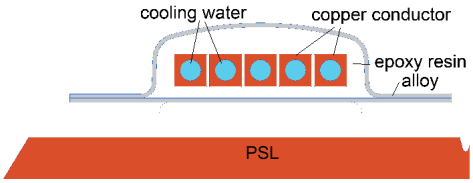

Fig. 2. Detail of the `B`-coil model

2.2. *Magnetic flux density*

The magnetic flux density B_n (component normal to the plane of the coil) is evaluated at 10 cm distance above the coils plane at the coil centre, corresponding to the surface of a typical ASDEX Upgrade plasma. Fig. 3 is a plot of B_n as a function of frequency for `Bu-` and `Bl-` coils with different distances d to the PSL. For `Bl-`coils, B_n is quite higher than for `Bu-`coil at the same current. This is due to larger eddy currents in the PSL at smaller distance. The corner frequency is at about 1.2 kHz, above which the produced field drops quickly. At $f = 500$ Hz and $I_{\mathrm{coil}} = 1$ kA, $B_n = 5.1$ mT (`Bl`) and 2.7 mT (`Bu`).

Figure 4 shows, that the induced eddy currents in the PSL not only reduce the magnitude of the field but also change the phase angle of the resulting flux with respect to the coil current. The phase angle of the current in the coil casing is smaller than the

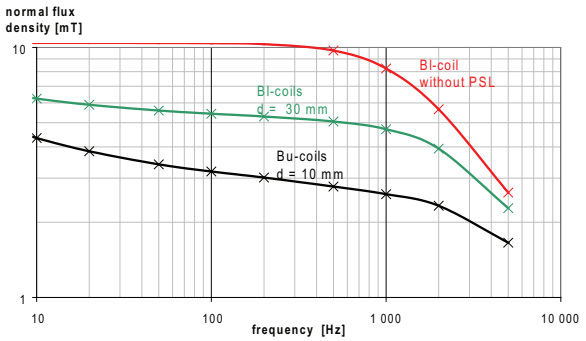

Fig. 3. Normal flux density B_n (magnitude) at the reference point produced by `B`-coils at $I_{\mathrm{peak}} = 1$ kA

[1] `www.quickfield.com`

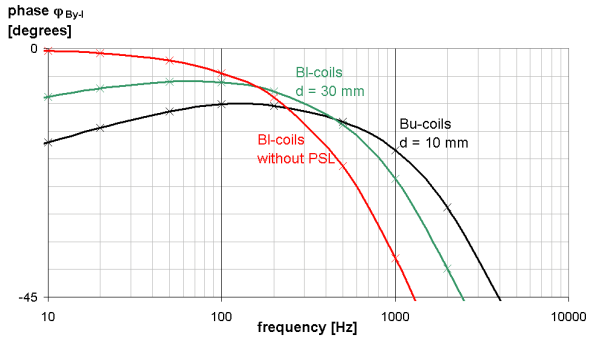

Fig. 4. Phase between normal field and applied coil current.

phase angle of the PSL current, which is about 180^0 to the coil current. This is due to the casing's higher resistance. Therefore at higher frequencies the casing has an stronger influence on the phase angle between coil current and flux than the PSL.

2.3. *Current density*

Figure 5 shows the current density pattern (sign suppressed) and field lines for 1 kA_{peak} coil current and $f = 1$ kHz. The skin effect in the copper conductors is clearly seen. The current peaks are at the edges of the copper winding and in particular at the surface facing towards the PSL where a maximum current density of 50 A_{rms}/mm^2 occurs. Noting that the PSL current has opposite phase of the winding current, this is identified as the well-known proximity effect in electrical machines. Furthermore, the current density in the top of the casing is slightly higher than in the bottom, close to the PSL.

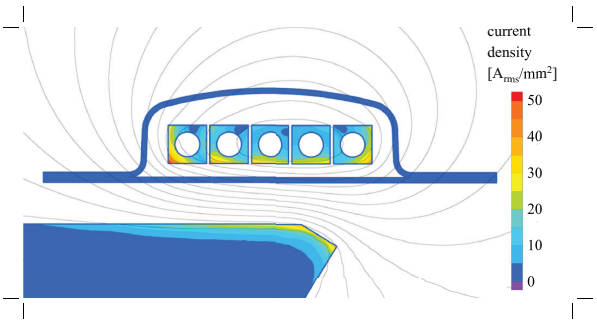

Fig. 5. Current density and field lines of `Bu`-coil at $I_{coil} = 1$ kA and $f = 1$ kHz.

2.4. *Load parameters*

Load parameters are important for the ac power supply design. Figure 6 shows that inductance and resistance strongly depend on frequency. The inductance decreases with rising frequency because the increasing eddy currents reduce the resulting flux. The resistance increases with increasing frequency because of the ohmic losses in the passive structures. In addition the current-carrying cross-section of the winding is reduced by the skin effect. These losses result in increasing active power consumption.

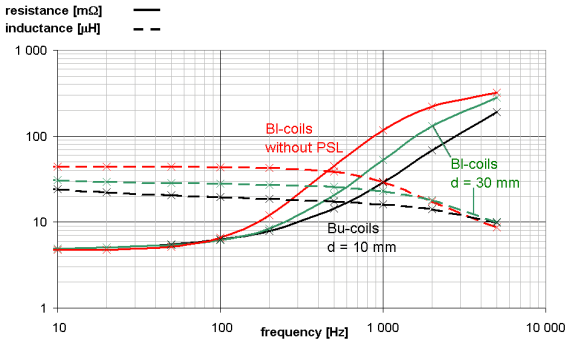

Fig. 6. Comparison of coil resistance R and inductances L

2.5. *Induced voltage and current during disruptions*

Disruptions are characterised by rapid changes of the flux (and hence induced voltages) in surrounding conductors by (a) the plasma current quench and (b) vertical displacement of the plasma column. If the coils are short-circuited, large coil currents result which lead to significant $j \times B$ forces on the coils. On the other hand, direct flow of halo currents into the coil casing is avoided because the protecting tiles towards the plasma are mounted on the PSL and have no direct electrical connection with the coils. Furthermore the coil casing is connected only at one bolt with the PSL and therefore cannot bypass PSL currents. We therefore consider the induced currents in the copper winding as the main origin of forces on the coils.

The maximum current during disruptions is assessed by 2D `Quickfield` simulations using the geometry shown in Fig. 7. A broad current distribution is assumed as indicated by the yellow region in the lower right corner of the figure. Current quench rate and vertical displacement velocity are taken from the disruption in shot 18 019, that would have in-

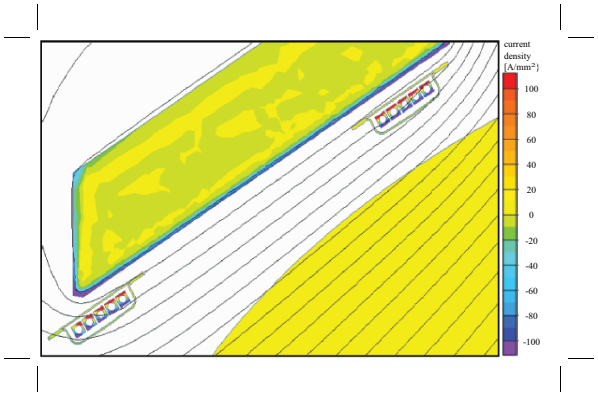

Fig. 7. Flux lines and induced current density in conductors during a "worst-case" disruption.

duced the highest voltage in the coils. The plasma current gradient in the model has been adapted to reach this fast change of flux in the coils. Without PSL, the maximum voltage between the two coil branches is 421 V. With PSL present in the model, the voltage difference reduces to 35 V.

The induced short circuit current amounts to 1.2 kA.

This vast reduction of induced voltage is largely due to image currents in the PSL. Because of the long PSL time constant (several 100 ms), the flux lines are almost parallel to the PSL surface, and hence there is little voltage drop over the coil winding which is parallel to the PSL (and mostly parallel to flux lines).

3. Thermal simulations

A first analytical estimate of the inductive heating of the coil casing is based on the equivalent circuit diagram. The coil (without PSL) is regarded as a transformer with the casing as a short circuited secondary winding and approximately no leakage inductance. This model is compared with the Joule heating rate calculated with `QuickField` for the given thermal capacity of the structures. Figure 8 shows (for `B`-coils without PSL) that the analytical model is in good qualitative agreement with the `QuickField` result.

3.1. *Joule heating of the coil casing*

The Joule heating rate $\mathrm{d}T/\mathrm{d}t$ of the modified coil design, taken at the hottest spot of the coil casing (the casing top), is shown in Fig. 8. At $f = 500$ Hz and $I_{\mathrm{coil,peak}} = 1$ kA, $\mathrm{d}T/\mathrm{d}t = 1.6$ K/s (`Bu`) and 3.2 K/s (`Bl`). For $\Delta T = 40$ K tolerable temperature swing, this corresponds to pulse lengths of $\Delta t = 25$ s and 12.5 s, respectively, which are beyond the ASDEX Upgrade pulse length and longer than the required pulse time of 6 seconds for the saddle coils. At $f = 1$ kHz (and $I_{\mathrm{coil,peak}} = 1$ kA), the pulse length drops to 7.3 s (`Bu` coils) and 3.7 s (`Bl` coils).

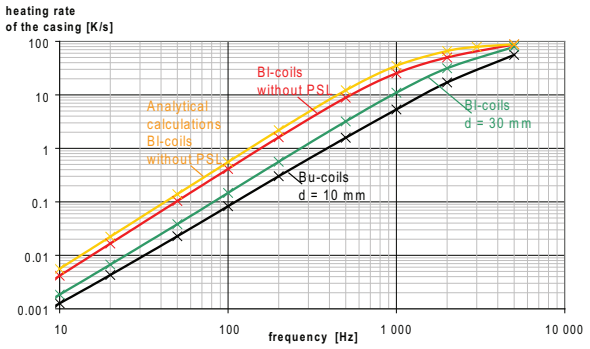

Fig. 8. Time-averaged heating rate of the coil housing for $I_{coil,peak} = 1\ kA$

3.2. *Inter-shot cooling of the coil casing*

The heat conduction problem is solved in 2D with the `QuickField` finite element code, using the same geometry as used for the electromagnetic calculations. The model treats heat conduction from the coil casing through the epoxy cast into the copper winding.

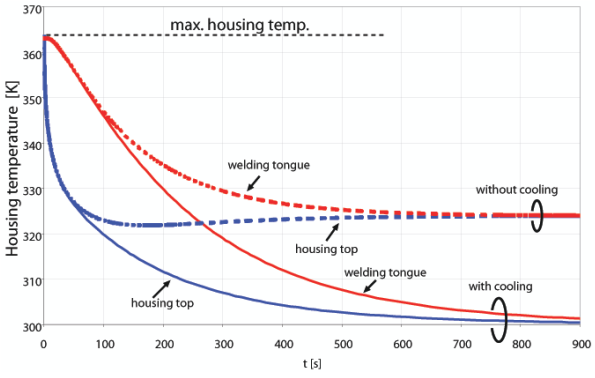

Fig. 9. Cool-down of coil casing top and welding tongue (with and without water cooling of the copper winding) starting from a homogeneous temperature of $T = 90°$C.

Fig. 9 shows the casing temperature during cool-down starting from a homogeneous temperature of $T = 90°$C in the coil casing (the maximum temperature tolerable for the epoxy casting). Without cool-

ing water flow in the copper conductor (i.e. no heat loss from the winding), the temperature in the coil equilibrates at about 52^{o}C (325 K). Active cooling is achieved by water flow in the copper conductor. The maximum cooling water temperature at ASDEX Upgrade is 27^{o}C (300 K), which is assumed to be the water temperature. For a tolerable temperature swing of 40 K as assumed above, the casing must cool to below 50^{o}C before a new pulse can be launched. This takes about 90 seconds for the coil top and 300 seconds for the welding tongue (the slowest component).

After 900 seconds (15 minutes, in practice the minimum time between pulses at ASDEX Upgrade) the entire coil has essentially cooled to the cooling water temperature, so no cumulative increase ("ratcheting") of the coil temperature is expected to occur.

4. Summary and conclusions

The electromagnetic simulations show that the saddle coils can be operated in a frequency range of dc ... 1 kHz. Table 1 shows a list of key parameters. The values achieved for both types of coils are better than the original requirements (column labelled "req") in all cases. The different behaviour of `B1`- and `Bu`-coils demonstrates the influence of the coil distance to the PSL (30 mm and 10 mm, respectively). The eddy currents in this massive copper conductor ($L/R \approx 600$ ms) lead to a reduction of the produced field in almost the entire frequency range. Dissipation in the PSL leads to a phase lag of the field with respect to the coil current Φ_{Bn-I}. This quantity is relevant for the phase margin of a closed loop for MHD stabilisation if the coil current is controlled (small signal response). The calculations show that the phase lag is less than 30^0 from dc up to 1 kHz which in practice leaves at least 120^0 phase margin for the remainder of the control loop.

The entire magnetic flux produced by the winding must penetrate the steel casing which therefore defines the corner frequency of the useful frequency range. We find $f_C = 1.2$ kHz for both types of coils. At high frequencies, power dissipation and heating in the casing set hard operational limits. At full coil current, $I_{\mathrm{coil,peak}} = 1$ kA, and $f = 1$ kHz, the real power input is $P = 18$ MW for a `Bu`-coil and 32 MW for a `B1`-coil. The corresponding casing heating rate at these parameters limits the pulse length to less than the ASDEX Upgrade pulse length. For a locked-mode avoidance scheme, the plasma control system must therefore begin to apply the fast rotating error field only if the risk of a locked-mode is actually detected and then take measures to remove the origin of the locked mode (e.g. reduce the plasma-β) while the rotating error field protects the plasma from the imminent disruption. The available pulse duration at full coil current and frequency of $t_{\mathrm{pulse}} = 3.7$ s is much larger than all characteristic plasma time scales and should therefore be sufficient to react.

High frequency operation of the inductors naturally implies significant apparent power, about $S = 50$ kVA at $I_{\mathrm{coil,peak}} = 1$ kA and $f = 1$ kHz for both types of coils. In order to reduce the apparent power for the entire coil set, each group of eight toroidally distributed coils can favourably be supplied with back-feeding inverters from one common dc link, so that for a rotating periodic signal, the coils can mutually exchange their magnetic energy. The reaction of a feedback controller to a fast growing mode, however, leads to simultaneously increasing reactive power to all coils. The power level and bandwidth depends on the mode growth rate and properties of the feedback system such as mutual inductance between coils and plasma mode, mode growth rate, dead time and phase shifts in the control loop. A stable system is expected to keep the mode amplitude and therefore the ac power at a low level. Details can only be assessed by modeling the full control system, including plasma, sensors, controller and power supplies, which is a next step in the design of an RWM control system.

References

[1] P. Anderson, C. Baxi, A. Kellman, E. Reis, Design, fabrication, installation, testing and initial results of in-vessel control coils for DIII-D, Fusion Science and Technology.

[2] G. Marchiori, M. Cavinato, R. Masiello, R. Paccagnella, Electromagnetic modeling for the active control of MHD modes in RFX, Fusion Engineering and Design.

[3] B. Giesen, O. Neubauer, E. Bondarchuk, N. Doinikov, B. Kitaev, T. Obidenko, A. Panin, Investigation of eddy currents in the components of the Dynamic Ergodic Divertor at TEXTOR using analytical and numerical approaches, 22nd SOFT, Helsinki.

[4] W. Suttrop, A. Herrmann, M. Rott, T. Vierle, U. Seidel, B. Streibl, D. Yadikin, O. Neubauer, B. Unterberg, E. Gaio, V. Toigo, P. Brunsell, the ASDEX Upgrade Team, In-vessel saddle coils for MHD control in ASDEX Upgrade, this conference.

Table 1
Required and achieved parameters (peak values for ac operation) for `Bl`-coils and `Bu`-coils at peak coil current $I_{\mathrm{coil}} = 1$ kA.

quantity			req.	achieved		units	conditions
				`Bl`	`Bu`		
dc normal field	Min.	B_n	6	9		mT	$f = 0$
Corner frequency	Min.	f_C	500	1200		Hz	
ac normal field	Min.	B_n	1	5.1	2.7	mT	$f = 500$ Hz
				4.7	2.6	mT	$f = 1$ kHz
Phase lag of field	Max.	Φ_{Bn-V}	150	90	90	deg.	$f \leq 500$ Hz
		Φ_{Bn-I}		≤ 18	≤ 30	deg.	$f \leq 1$ kHz
Peak coil voltage	Max.	V_{coil}	500	188	131	V	$f = 1$ kHz
Pulse duration	Min.	t_{pulse}	6	12.5	27	s	$f = 500$ Hz
				3.7	7.3	s	$f = 1$ kHz
Cool-down time	Max.	t_{pause}	900	< 100		s	$\Delta T = 40$ K

[5] T. Vierle, B. Streibl, M. Rott, U. Seidel, A. Herrmann, O. Neubauer, W. Suttrop, the ASDEX Upgrade Team, Design and stress analysis of in-vessel saddle coils for MHD control in ASDEX Upgrade, this conference.

[6] E. Philippow (Ed.), Taschenbuch Elektrotechnik, 3rd Edition, Vol. 1, Carl Hanser Verlag, 1986.

[7] P. Martin, H. Preis, Programmbeschreibung und Benutzeranleitung zum Magnetfeld–Computer–Programm HEDO 2, Tech. rep., Max-Planck-Institut für Plasmaphysik, IPP-Report III/34 (1977).